INSTITUTE OF PHYSICS PUBLISHING PHYSICS IN MEDICINE AND BIOLOGY

Phys. Med. Biol. **51** (2006) 3593–3602 doi:10.1088/0031-9155/51/14/021

Evaluation of response to treatment using DCE-MRI: the relationship between initial area under the gadolinium curve (IAUGC) and quantitative pharmacokinetic analysis

S Walker-Samuel, M O Leach and D J Collins

Cancer Research UK Clinical Magnetic Resonance Imaging Research Group, Royal Marsden & NHS Foundation Trust and Institute of Cancer Research, Belmont, Surrey SM2 5PT, UK

E-mail: simon.walker@icr.ac.uk

Received 1 March 2006, in final form 25 May 2006
Published 6 July 2006
Online at stacks.iop.org/PMB/51/3593

Abstract

The initial area under the gadolinium curve (IAUGC) is often used in addition to or as an alternative to parameters derived from pharmacokinetic modelling of T_1-weighted dynamic contrast-enhanced (DCE) MRI data in the assessment of response to treatment of cancer. However, the physiological meaning of the IAUGC has not been rigorously defined with respect to model-based parameters. Here, simulations of DCE-MRI data were used to investigate the relationship between IAUGC and the parameters K^{trans} (transfer constant), v_e (fractional extravascular extracellular volume) and v_p (fractional plasma volume), using two vascular input functions. It is shown that IAUGC is a mixed parameter that can display correlation with K^{trans}, v_e and v_p and ultimately has an intractable relationship with all three. Furthermore, it is demonstrated that the range over which IAUGC is taken and the nature of the vascular input function do not significantly affect this relationship.

Introduction

A recent workshop report (Leach *et al* 2003) made recommendations on the use of MRI methods to assess anti-angiogenic and anti-vascular drugs to treat cancer. An emphasis was placed on the use of dynamic contrast-enhanced (DCE) MRI measurements, which included advice on the use of 'quantitative' and 'semi-quantitative' parameters. The former includes parameters such as the vascular transfer constant (K^{trans}) and extra-vascular extra-cellular space (v_e), whereas examples of the latter include the initial area under the gadolinium curve (IAUGC), peak enhancement and initial wash-in gradient. The terms 'semi-quantitative' and 'quantitative' can be misleading, as 'semi-quantitative' parameters can be fully quantitative, in that they can be measured objectively and reproducibly. The distinction between parameters

such as IAUGC and model-based parameters tends to be the latent dependency of non-model-based parameters on physiological processes. Yet this division can also be blurred if a physiological basis for these measures were to be deduced. For these reasons, the terms 'model-based' and 'non-model-based' shall be employed in place of 'quantitative' and 'semi-quantitative'. Furthermore, the term 'pharmacokinetic analysis' will refer to the iterative fitting of a model function with parameters based on known physiological processes.

Therapeutic response due to anti-cancer drugs is usually assessed using sequential measurements. One or more baseline measurements are acquired followed by post-treatment measurements. A number of studies have investigated the correlation between the magnitude of change of model-based parameters following therapy and clinical response criteria or drug retention (Su *et al* 2002, Baba *et al* 1997, Padhani *et al* 2001, Morgan *et al* 2003, Jayson *et al* 2002), VEGF expression in osteosarcoma (Hoang *et al* 2004) and prostate tumour stage (Padhani *et al* 2000). However, in order to avoid some of the challenges associated with pharmacokinetic modelling (such as computational expense, post-processing inaccuracies, fit failures, etc), non-model-based parameters are often used in addition to or in place of model-based parameters (Hawighorst *et al* 1999, Galbraith *et al* 2002, Leach *et al* 2005, Evelhoch 1999). Changes in IAUGC and other non-model-based measures (such as peak enhancement, wash-in gradient, etc) have been shown to correlate with tumour regression rate in cervical carcinoma during radiotherapy (Gong *et al* 1999) and both the staging (Padhani *et al* 2000) and the discrimination of prostate cancer from normal tissue (Engelbrecht *et al* 2003). However, the biological relevance of many commonly used non-model-based parameters has not been defined, thereby limiting the interpretation of their absolute values or relative variations in terms of the underlying physiology. Evelhoch *et al* suggested that IAUGC relates to blood flow, vascular permeability and the fraction of interstitial space, but did not qualify the nature of this relationship. Parker and Buckley (2005) state that IAUGC is a 'measure of the amount of contrast agent delivered to and retained within the tumour within the stated time period', which amounts to the definition. Furthermore, studies *in vivo* have suggested a strong correlation between IAUGC and fraction of interstitial space (Walker *et al* 2003). With the widespread clinical use of IAUGC in mind, it is clear that the relationship between IAUGC and the physiological mechanisms of contrast enhancement must be more clearly defined.

The current study therefore aimed to characterize the relationship between IAUGC and model-based parameters. As no gold standard *in vivo* measurement of the model-based parameters in question exists, this analysis was performed numerically using simulated DCE-MRI data. There is much debate regarding the suitability of various estimates of the plasma Gd-DTPA concentration used in pharmacokinetic analysis (Harrer *et al* 2004), so two different vascular input functions (VIFs) were used in the analysis. Furthermore, a range of temporal periods over which the IAUGC should be calculated have been reported (Leach *et al* 2003). Three temporal ranges were therefore evaluated in this study.

Theoretical background

Dynamic contrast-enhanced (DCE) MRI is frequently used in a clinical setting to monitor the passage of a bolus of a contrast agent such as Gd-DTPA through the body. The presence of contrast agent *in vivo* induces an increase in the longitudinal relaxation rate ($R_1 = 1/T_1$) of water in proportion to the concentration of the contrast agent, resulting in an increase in the signal intensity measured using a suitably weighted acquisition sequence. Gd-DTPA is able to traverse the vascular endothelium and enter the extracellular extravascular space (EES), but is unable to cross the cellular membrane, so provides a mechanism by which the dynamics of exchange between the capillary bed and the EES can be evaluated.

The pharmacokinetics of Gd-DTPA *in vivo* are usually modelled as a two-compartment system, consisting of the vascular space and the EES. Tissue contrast agent concentration, C_t, as a function of time, t, is modelled using the modified Kety equation (Tofts *et al* 1999):

$$\frac{\mathrm{d}C_t(t)}{\mathrm{d}t} = K^{\mathrm{trans}} C_\mathrm{p}(t) - k_\mathrm{ep} C_t(t). \tag{1}$$

This characterizes exchange from the vasculature into the EES and back from the EES in to the vasculature with the rate constants K^{trans} and k_ep, respectively. It requires an estimate of the blood plasma contrast agent concentration, C_p, which is often referred to as the vascular input function (VIF). The most general definition of $\mathrm{K}^{\mathrm{trans}}$ is

$$K^{\mathrm{trans}} = (1 - \mathrm{e}^{-PS/F(1-\mathrm{Hct})}) F\rho(1 - \mathrm{Hct}), \tag{2}$$

where PS is the permeability surface area product per unit mass of tissue (ml min^{-1} g^{-1}), F is the flow of blood per unit mass of tissue (ml min^{-1} g^{-1}), Hct is the haematocrit fraction and ρ is the tissue density (g ml^{-1}).

Most models used to analyse DCE-MRI data are derived from the modified Kety equation. One of the most widely used is the Tofts and Kermode model, which assumes that C_p can be characterized by a bi-exponential decay of the form

$$C_\mathrm{p}(t) = D(a_1 \mathrm{e}^{-m_1 t} + a_2 \mathrm{e}^{-m_2 t}), \tag{3}$$

where a_1 and m_1 relate to exchange between blood plasma and the EES throughout the whole body and a_2 and m_2 relate to the slower extraction rate by the kidneys (Tofts and Kermode 1991). A standard set of a_i and m_i is usually used in the Tofts and Kermode model, which were derived from studies of Gd-DTPA *in vivo* (Tofts and Kermode 1991, Weinmann *et al* 1984).

If equation (3) is substituted into equation (1), the following solution can be derived (Tofts and Kermode 1991), which constitutes the Tofts and Kermode model:

$$C_t(t) = DK^{\mathrm{trans}} \sum_{i=0}^{2} a_i \frac{(\mathrm{e}^{-k_\mathrm{ep} t} - \mathrm{e}^{-m_1 t})}{m_i - k_\mathrm{ep}}. \tag{4}$$

The fractional size of the EES, v_e, can be calculated from parameters in the Tofts and Kermode model by the simple relationship $v_\mathrm{e} = K^{\mathrm{trans}}/k_\mathrm{ep}$. A criticism of the Tofts and Kermode model is its assumption of negligible blood plasma fraction, v_p. An extra term can be added to equation (4) to take this into account, resulting in the extended Tofts and Kermode model (Tofts 1997):

$$C_t(t) = DK^{\mathrm{trans}} \sum_{i=0}^{2} a_i \frac{(\mathrm{e}^{-k_\mathrm{ep} t} - \mathrm{e}^{-m_1 t})}{m_i - k_\mathrm{ep}} + v_\mathrm{p} C_\mathrm{p}(t). \tag{5}$$

Methods and materials

The integral of equation (4) with respect to time is a complicated function with no obvious, simple approximation for its dependence on K^{trans} or v_e, so the relationships between IAUGC and each model-based parameter were evaluated numerically. Approximately 4000 contrast agent uptake curves were simulated using the extended Tofts and Kermode model (equation (5)) using two estimates for the VIF.

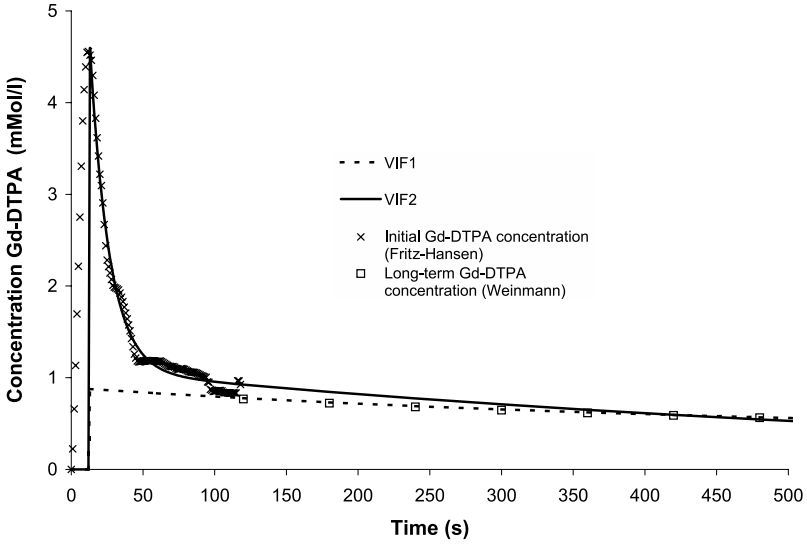

Figure 1. Graphs of the bi-exponential VIFs as functions of time used in the Tofts and Kermode model. The dashed line corresponds to VIF1, which was derived from the data of Weinmann *et al* (1984) and the solid line corresponds to VIF2, derived from data acquired by both Weinmann *et al* and Fritz-Hansen *et al* (1996). To derive VIF2, the average aorta Gd-DTPA plasma concentration was taken from six measurements published by Fritz-Hansen *et al*, with measurements by Weinmann *et al* concatenated at $t > 3$ min. The peak concentration value was identified and data following it were fitted with a bi-exponential function.

Vascular input functions

The first VIF (VIF1) was composed of the bi-exponential curve fitted by Tofts and Kermode (1991), of the from of equation (3), to Gd-DTPA extraction data measured by (Weinmann *et al* 1984) ($a_1 = 3.99$ kg l^{-1}, $m_1 = 0.144$ min^{-1}, $a_2 = 4.78$ kg l^{-1}, $m_2 = 0.011$ min^{-1}). Administration of a single dose ($D = 0.1$ mmol kg^{-1}) of Gd-DTPA was simulated. This VIF is commonly used in pharmacokinetic modelling, but does not characterize the first pass of contrast agent observed in high temporal resolution studies (<20 s) prior to mixing or equilibration of the bolus in the plasma compartment.

The second VIF (VIF2) was derived from data published by Fritz-Hansen *et al* (1996), in which the whole-blood concentration of Gd-DTPA in the aorta was measured for a duration of approximately 120 s, at high temporal resolution. During the current study, the aortic concentration–time curves from all patients featured in the Fritz-Hansen *et al* study were input to a computer using a digital scanner and software was developed to identify the data points in each. Each curve was interpolated using a cubic spline and the onset times of each curve were identified and aligned. The mean concentration value at each time point was calculated to produce an averaged uptake curve. To convert from whole-blood to blood plasma concentration, this averaged curve was scaled by $1/(1 - \mathrm{Hct})$, where Hct is the haematocrit fraction, taken as 0.45. In order to characterize Gd-DTPA concentration for time points greater than 120 s, VIF1 was reconstructed with a temporal resolution of 60 s and appended to the data. A bi-exponential function of the form given by equation (3) was fitted to these aggregate data following peak concentration (see figure 1). Whilst this VIF approximates the aorta concentration as bi-exponential in form (and can therefore be incorporated into the Tofts and Kermode model), it describes the first pass of contrast agent more accurately than VIF1 and is therefore more suited to high temporal resolution measurements.

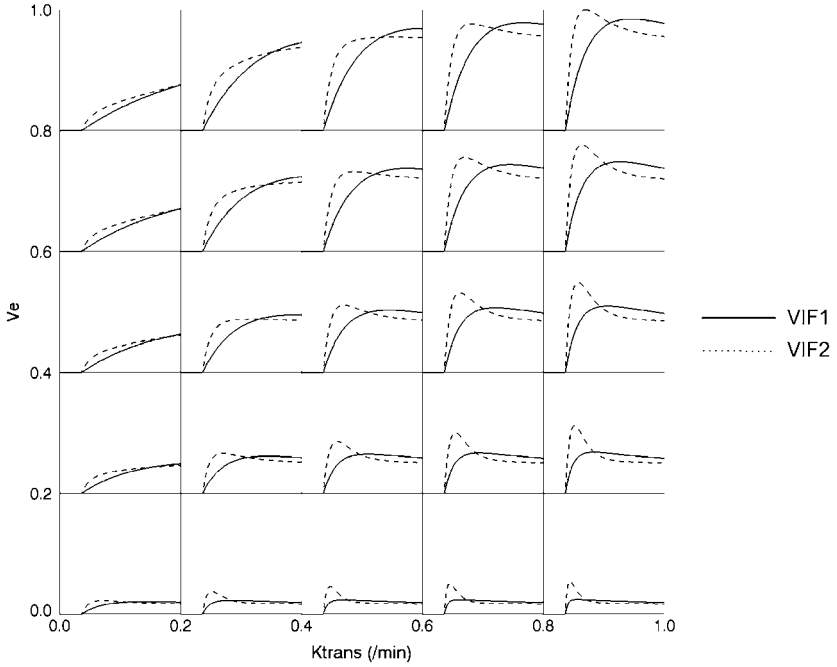

Figure 2. Simulated contrast agent uptake curves plotted as functions of time, positioned relative to their K^{trans} and v_e values. The total duration of the curves is 800 s, with onset at 60 s. Curves simulated using VIF1 and VIF2 are shown with solid and dashed lines, respectively.

Simulation parameters

Each simulated curve was assigned a unique value of K^{trans} and v_e, which were varied uniformly in the range 0–1 min^{-1} and 0–1, respectively. v_e can only vary between 0 and 1 as it represents the fractional extracellular extravascular space, but K^{trans} could, in theory, take a value of greater than 1.0 min^{-1}. However, this would require unrealistically large vascular flow values. The temporal resolution of the data sampling for the simulation of the curves was set to 5 s and total duration 500 s, which are typical of data acquired *in vivo*. All simulations were programmed in IDL (RSI, Boulder, CO). IAUGC was calculated for each curve within the limits 0–60 s, 0–90 s and 0–180 s (denoted IAUGC60, IAUGC90 and IAUGC180, respectively) using a five-point Newton–Cotes integration formula (Press *et al* 1988). Note that 0 s corresponds to the onset time of contrast agent.

Results

Figure 1 shows VIF1 and VIF2 as functions of time. This graph clearly shows the first pass of contrast agent in VIF2 that is not found in VIF1 and their equivalence following the first pass. The fitting of a bi-exponential function to the combined initial and long-term concentration data resulted in the following parameters: $a_1 = 36 \pm 1$ kg l^{-1}, $m_1 = 4.9 \pm 0.1$ min^{-1}, $a_2 = 13 \pm 1$ kg l^{-1}, $m_2 = 0.23 \pm 0.08$ min^{-1}.

Figure 2 shows examples of the simulated concentration–time curves, positioned with respect to their K^{trans} and v_e values, for both VIFs. For these simulations, v_p was kept constant

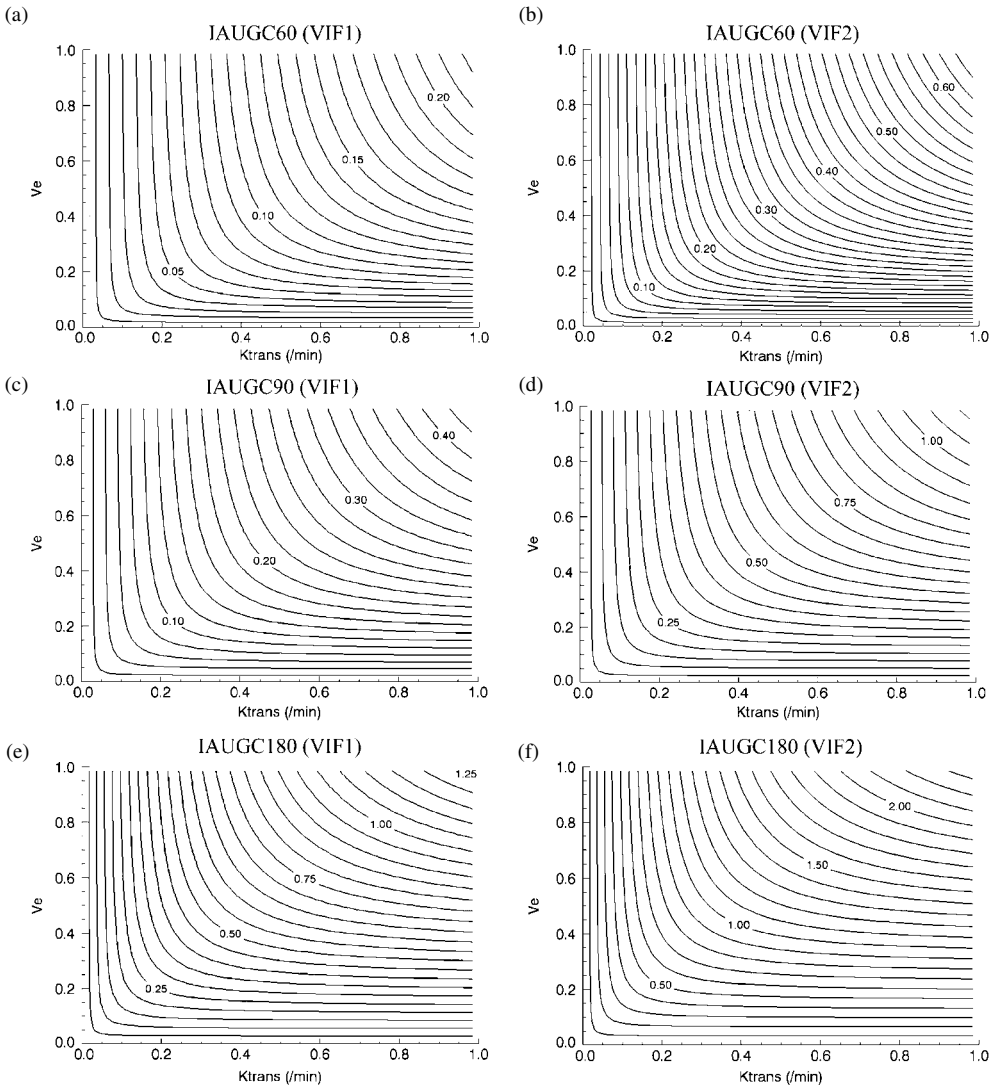

Figure 3. Contour plots of IAUGC from curves simulated using VIF1 (a), (c) and (e) and VIF2 (b), (d) and (f), as functions of K^{trans} and v_e for three ranges: IAUGC60 (a) and (b), IAUGC90 (c) and (d) and IAUGC180 (e) and (f). The value of v_p was set at 0.01 in all plots. Contour labels denote the value of IAUGC in mmol min l^{-1}. Note that the spacing between contours varies between plots.

at 0.01, as this is a typical value found *in vivo* (Weissleder *et al* 1998, Wang *et al* 1998). Visual inspection of the curves suggests that v_e has the main influence on the level of enhancement of the curves, yet this effect decreases with increasing K^{trans}. Furthermore, increasing K^{trans} causes the first-pass effect in VIF2 to become more evident in the uptake curves, thereby increasing the initial peak enhancement for a given value of v_e.

Figure 3 shows contour plots of IAUGC, for each VIF, as functions of K^{trans} and v_e. Again, v_p was kept constant at 0.01. All IAUGC distributions show the same trend: they are low in magnitude for small v_e (bottom of the graph) and small K^{trans} (left-hand side)

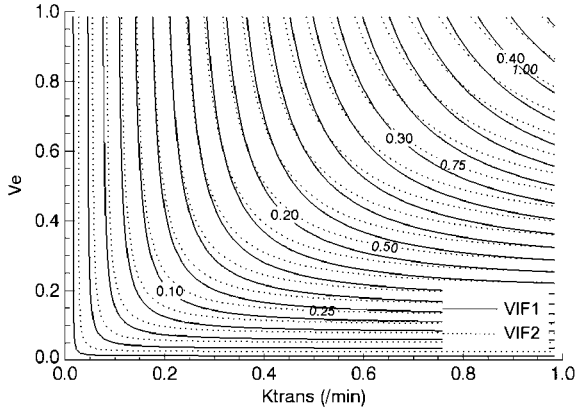

Figure 4. Contour plot of IAUGC90 as a function of K^{trans} and v_e for VIF1 (solid line) and VIF2 (dotted line).

and large in magnitude for large K^{trans} and v_e (top right-hand corner). The orientation of the contours suggests that for 'large' K^{trans} and 'small' v_e, IAUGC is proportional to v_e (horizontal contours) and for 'small' K^{trans} and 'large' v_e, IAUGC is proportional to K^{trans} (vertical contours). How large or small each parameter has to be in order to correlate with IAUGC depends on the range over which IAUGC is taken. For example, IAUGC180 tends towards correlation with v_e (horizontal contours in figure 3(e)) over a larger range of K^{trans} compared with IAUGC60. Generally, figure 3 indicates that the larger the range of IAUGC, the more likely it is to correlate with v_e for the given range of K^{trans}.

Figure 3 also shows that IAUGC values derived using VIF1 and VIF2 display the same qualitative relationship with v_e and K^{trans}. The main difference is simply that VIF2 gives larger values of IAUGC. The dependence of IAUGC90 on K^{trans} and v_e for both VIFs is shown in figure 4, which illustrates the slight differences in the regions over which IAUGC is proportional to either K^{trans} or v_e.

The introduction of a blood volume term in the extended Tofts and Kermode model introduces an offset into the distribution of IAUGC, the value of which depends solely on v_p and $C_p(t)$. Figure 5 shows surface plots of the variation of IAUGC with K^{trans} and v_e for four values of v_p. The shape of the surface for each value of v_p does not change—they are simply offset by a value proportional to $v_p \int_0^\tau C_p(\tau)\,d\tau$ where τ is the top limit of the IAUGC range.

Discussion and conclusions

In this study, we numerically evaluated the relationship between IAUGC and the model parameters K^{trans}, v_e and v_p, using two different VIFs. IAUGC is often used clinically in addition to or in preference to physiological parameters due to its robustness, lack of assumptions and ease of implementation. However, the physiological relevance of IAUGC has not previously been clearly defined and the physiological meaning of a change in such a parameter (such as might be found following treatment for cancer) is unknown.

The simulations performed during this study showed that IAUGC is a mixed parameter in terms of K^{trans} and v_e and that IAUGC can be directly correlated with either K^{trans} or v_e, in restricted regions of a contour plot such as those shown in figure 3. Furthermore, the addition of a v_p term adds (see figure 5) further complexity to the relationship, even though its effect

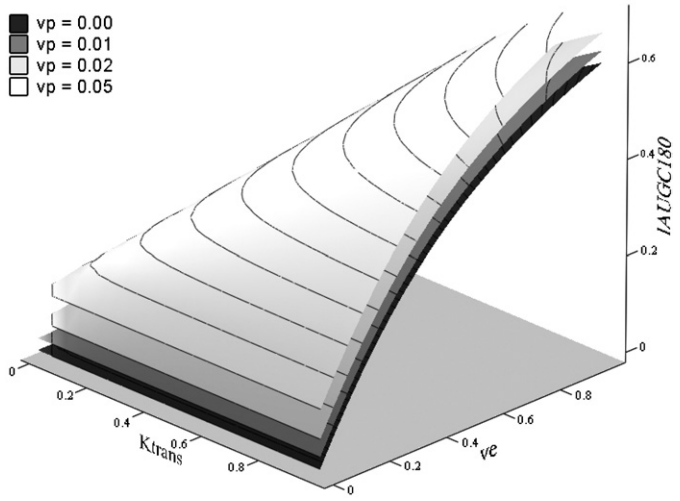

Figure 5. Surface plots showing the dependence of IAUGC on K^{trans} and v_e for four values of v_p: 0.0, 0.01, 0.02 and 0.05.

is simply to add a positive offset to the IAUGC. As shown by comparing figures 3(a), (c) and (e), the range over which IAUGC is taken affects its magnitude (IAUGC180 for a given curve is greater than IAUGC90 for example), but has little bearing on its relationship with K^{trans} and v_e. No additional insights into tissue physiology are gained by investigating IAUGC over different ranges. However, a larger range of IAUGC has a greater signal-to-noise advantage as the number of time points that are averaged increases. It can therefore be reasoned that the range that IAUGC is taken over is unimportant as long as it is long enough to ensure good signal-to-noise and is used consistently in order to acquire IAUGC values with comparable magnitudes between studies. IAUGC90 is commonly calculated *in vivo* and could therefore be recommended as a standardized parameter.

Two bi-exponential VIFs were used in this study: VIF1 described the plasma contrast agent kinetics once the bolus has become well mixed, whereas VIF2 included a first-pass phase (figure 1). The differences evident in the contour plots of IAUGC in figure 3 for VIF1 and VIF2 (for example figures 3(a) and (b)) are minimal in terms of the relationship of IAUGC with K^{trans} and v_e; the main difference is that the magnitude of IAUGC is greater for VIF2. However, this does not mean that IAUGC is independent of VIF used, rather that the relationship with K^{trans} and v_e, for the two VIFs studied here, is independent of a_i and m_i in equation (3). As VIF1 and VIF2 are representative of the Gd-DTPA plasma distribution *in vivo*, this suggests that the relationship between IAUGC and K^{trans} and v_e defined here can be assumed to apply to most *in vivo* measurements using a bolus administration of Gd-DTPA. It should be noted, however, that these relationships may not hold for significantly different contrast agent delivery protocols (such as an infusion).

It is clear from figure 3 that a number of biological properties can account for a particular IAUGC value. For example, the IAUGC90 = 0.10 mmol min l^{-1} contour in figure 3(c) could be associated with a K^{trans} value anywhere from 0.15 to at least 1.0 min^{-1} and v_e from 0.1 to 1.0. Clearly, IAUGC cannot be used as a surrogate measure of either K^{trans} or v_e. Reversing this argument requires that a measured change in IAUGC following therapy could correspond to a variety of physiological changes. Furthermore, in practical terms, a general change in

tissue physiology could be understated by IAUGC if it were to occur approximately along an IAUGC contour or overstated if orthogonal to a contour.

The findings discussed here imply that IAUGC can only be interpreted according to the description provided by Parker and Buckley (2005): IAUGC is a measure of the amount of contrast agent delivered to and retained by the tumour in the given time period. This is a simple and fundamental measure, but only summarizes what is already known: the concentration of contrast agent as a function of time. It has the advantage of good signal-to-noise characteristics, but the disadvantage that the physiological mechanisms mediating contrast agent concentration are intractable.

Acknowledgment

This work was supported by Cancer Research UK (C1060/A808/G7643).

References

Baba Y, Furusawa M, Murakami R, Yokoyama T, Sakamoto Y, Nishimura R, Yamashita Y, Takahashi M and Ishikawa T 1997 Role of dynamic MRI in the evaluation of head and neck cancers treated with radiation therapy *Int. J. Radiat. Oncol. Biol. Phys.* **37** 783–7

Engelbrecht M R, Huisman H J, Laheij R J, Jager G J, van Leenders G J, Hulsbergen-Van De Kaa C A, de la Rosette J J, Blickman J G and Barentsz J O 2003 Discrimination of prostate cancer from normal peripheral zone and central gland tissue by using dynamic contrast-enhanced MR imaging *Radiology* **229** 248–54

Evelhoch J L 1999 Key factors in the acquisition of contrast kinetic data for oncology *J. Magn. Reson. Imaging* **10** 254–9

Fritz-Hansen T, Rostrup E, Larsson H B, Sondergaard L, Ring P and Henriksen O 1996 Measurement of the arterial concentration of Gd-DTPA using MRI: a step toward quantitative perfusion imaging *Magn. Reson. Med.* **36** 225–31

Galbraith S M, Lodge M A, Taylor N J, Rustin G J, Bentzen S, Stirling J J and Padhani A R 2002 Reproducibility of dynamic contrast-enhanced MRI in human muscle and tumours: comparison of quantitative and semi-quantitative analysis *NMR Biomed.* **15** 132–42

Gong Q Y, Brunt J N, Romaniuk C S, Oakley J P, Tan L T, Roberts N, Whitehouse G H and Jones B 1999 Contrast enhanced dynamic MRI of cervical carcinoma during radiotherapy: early prediction of tumour regression rate *Br. J. Radiol.* **72** 1177–84

Harrer J U, Parker G J, Haroon H A, Buckley D L, Embelton K, Roberts C, Baleriaux D and Jackson A 2004 Comparative study of methods for determining vascular permeability and blood volume in human gliomas *J. Magn. Reson. Imaging* **20** 748–57

Hawighorst H, Libicher M, Knopp M V, Moehler T, Kauffmann G W and Kaick G 1999 Evaluation of angiogenesis and perfusion of bone marrow lesions: role of semiquantitative and quantitative dynamic MRI *J. Magn. Reson. Imaging* **10** 286–94

Hoang B H, Dyke J P, Koutcher J A, Huvos A G, Mizobuchi H, Mazza B A, Gorlick R and Healey J H 2004 VEGF expression in osteosarcoma correlates with vascular permeability by dynamic MRI *Clin. Orthop.* **426** 32–8

Jayson G C *et al* 2002 Molecular imaging and biological evaluation of HuMV833 anti-VEGF antibody: implications for trial design of antiangiogenic antibodies *J. Natl Cancer Inst.* **94** 1484–93

Leach M O *et al* 2003 Assessment of antiangiogenic and antivascular therapeutics using MRI: recommendations for appropriate methodology for clinical trials *Br. J. Radiol.* **76** (Suppl 1) S87–91

Leach M O *et al* 2005 The assessment of antiangiogenic and antivascular therapies in early-stage clinical trials using magnetic resonance imaging: issues and recommendations *Br. J. Cancer* **92** 1599–610

Morgan B *et al* 2003 Dynamic contrast-enhanced magnetic resonance imaging as a biomarker for the pharmacological response of PTK787/ZK 222584, an inhibitor of the vascular endothelial growth factor receptor tyrosine kinases, in patients with advanced colorectal cancer and liver metastases: results from two phase I studies *J. Clin. Oncol.* **21** 3955–64

Padhani A R, Gapinski C J, Macvicar D A, Parker G J, Suckling J, Revell P B, Leach M O, Dearnaley D P and Husband J E 2000 Dynamic contrast enhanced MRI of prostate cancer: correlation with morphology and tumour stage, histological grade and PSA *Clin. Radiol.* **55** 99–109

Padhani A R, MacVicar A D, Gapinski C J, Dearnaley D P, Parker G J, Suckling J, Leach M O and Husband J E 2001 Effects of androgen deprivation on prostatic morphology and vascular permeability evaluated with MR imaging *Radiology* **218** 365–74

Parker G J and Buckley D L 2005 *Dynamic Contrast-Enhanced Magnetic Resonance Imaging in Oncology* (Heidelberg: Springer) pp 81–92

Press W H, Teukolsky S A, Vettering W T and Flannery B P 1988 *Numerical Recipes in C* 2nd edn (Cambridge: Cambridge University Press)

Su M Y, Yu H, Chiou J Y, Wang J, Nalcioglu O, Fruehauf J P, Mehta R S and Baick C H 2002 Measurement of volumetric and vascular changes with dynamic contrast enhanced MRI for cancer therapy monitoring *Technol. Cancer Res. Treat.* **1** 479–88

Tofts P S 1997 Modeling tracer kinetics in dynamic Gd-DTPA MR imaging *J. Magn. Reson. Imaging* **7** 91–101

Tofts P S *et al* 1999 Estimating kinetic parameters from dynamic contrast-enhanced $T(1)$-weighted MRI of a diffusable tracer: standardized quantities and symbols *J. Magn. Reson. Imaging* **10** 223–32

Tofts P S and Kermode A G 1991 Measurement of the blood–brain barrier permeability and leakage space using dynamic MR imaging: 1. Fundamental concepts *Magn. Reson. Med.* **17** 357–67

Walker S, Dzik-Jurasz A S, d'Arcy J A, Leach M O and Collins D J 2003 Evaluation of area under curve [Gd] data derived from DCE-MRI time series in brain tumours *International Society of Magnetic Resonance Imaging in Medicine (Toronto)*

Wang Z, Su M Y and Nalcioglu O 1998 Measurement of tumor vascular volume and mean microvascular random flow velocity magnitude by dynamic Gd-DTPA-albumin enhanced and diffusion-weighted MRI *Magn. Reson. Med.* **40** 397–404

Weinmann H J, Laniado M and Mutzel W 1984 Pharmacokinetics of Gd-DTPA/dimeglumine after intravenous injection into healthy volunteers *Physiol. Chem. Phys. Med. NMR* **16** 167–72

Weissleder R, Cheng H C, Marecos E, Kwong K and Bogdanov A J 1998 Non-invasive *in vivo* mapping of tumour vascular and interstitial volume fractions *Eur. J. Cancer* **34** 1448–54